Environmental Science
Water Research & Technology

PAPER

View Article Online
View Journal | View Issue

Cite this: *Environ. Sci.: Water Res. Technol.*, 2022, **8**, 2614

Surface functionalized poly(vinyl alcohol)–hydrous zirconium oxide composite beads for efficient and selective sequestration of phosphate from wastewater†

Huayong Luo,[a] Mingxuan Zhang,[a] Hongwei Rong,[a] Zuhao Chen,[a] Xueyang Zeng,[a] Jingyin Wang,[a] Binhua Liu[a] and Peng Liao *[b]

Received 1st June 2022,
Accepted 24th August 2022

DOI: 10.1039/d2ew00412g

rsc.li/es-water

The utilization of hydrous zirconium oxide (HZO) to sequester phosphate with good affinity and selectivity poses a significant challenge due to agglomeration and difficult separation. We envision that the simultaneous formation of HZO and host framework is an emerging strategy to improve the accessibility of HZO for phosphate capture. In this study, we reported a facile protocol for the synthesis of HZO encapsulated in crosslinked poly(vinyl alcohol) hydrogel beads (HZO-PVA) based on the simultaneous generation of HZO and cross-linking of PVA chains as a host. The resultant HZO-PVA can be further functionalized with triethylenetetramine (TETA@HZO-PVA) for effective and selective sequestration of phosphate. Specifically, batch experiments showed that TETA@HZO-PVA had better sequestration capacity towards phosphate than HZO-PVA, which was intimately related to the functionality of TETA that created a high density of surface binding sites. Additionally, TETA@HZO-PVA exhibited a great selectivity for phosphate even in the presence of competing anions and dissolved organic matter. Moreover, regeneration tests showed that TETA@HZO-PVA exhibited high reusability during five cycles of adsorption–desorption processes. Combined with characterization techniques and experiments, we identified that electrostatic attraction, ligand exchange, and Lewis acid–base interactions are the dominant mechanisms responsible for phosphate sequestration. Further, fixed-bed column experiments showed excellent phosphorus sequestration performance in real wastewater, making TETA@HZO-PVA a promising material for phosphorus sequestration in practical application.

Water impact

The issue of eutrophication posed by phosphorus pollution is one of the greatest water security challenges of the twenty-first century. We report surface functionalized poly(vinyl alcohol)–hydrous zirconium oxide composite beads that are inexpensive and can selectively sequestrate phosphate from real wastewater in a fixed-bed column, expanding the scope of application of zirconium-based materials for phosphate sequestration in wastewater.

1. Introduction

The issue of eutrophication posed by phosphorus (P) pollution continues to be one of the greatest water security challenges of the twenty-first century.[1,2] Adsorption is a simple and less labor-intensive technique that can sequestrate phosphorus so as to protect drinking-water supplies and reduce eutrophication on a global scale.[2–6] The development of material-based nanoparticles with superior adsorption and regeneration capacity can enhance phosphorus removal and facilitate the recovery of phosphorus using a suitable regeneration solution.[7,8] Zirconium based oxides have emerged as superior adsorbents for phosphate sequestration from aqueous solution due to their non-toxicity, good resistance to oxidizing agents and acids/bases, high thermal stability, and very low solubility in water.[9,10] Hydrous zirconia exists in an amorphous form, providing more hydroxyl groups on its surface and a higher surface area than crystalline zirconia because of its porous

[a] *School of Civil Engineering, Guangzhou University, Guangzhou, 510006, China*
[b] *State Key Laboratory of Environmental Geochemistry, Institute of Geochemistry, Chinese Academy of Sciences, Guiyang, 550081, PR China.*
E-mail: liaopeng@mail.gyig.ac.cn

† Electronic supplementary information (ESI) available. See DOI: https://doi.org/10.1039/d2ew00412g

and highly hydrated structure, showing more effectiveness in capturing anionic pollutants such as phosphate.[9,10] Rodrigues *et al.*[11] investigated hydrous zirconium oxide (HZO) for adsorption of Cr(VI) from aqueous solution, and found that HZO exhibited a surface area of 254 m^2 g^{-1}, higher than 78.1 m^2 g^{-1} observed on aluminium oxide for Cr(VI) removal, and 185 m^2 g^{-1} reported for Cr(VI) removal onto hydrous titanium oxide.[11] Though hydrated ferric oxide (HFO) has been extensively studied and widely used in phosphate removal due to its satisfactory capacity and relatively low operation cost, HFO is unstable and can dissolve under acidic conditions.[12] The potential secondary pollution from Fe leaching into waters would exert an adverse effect on organisms.[12] However, the fine morphology structure of HZO nanoparticles suffers from many challenges including aggregation, leaching, difficult separation, and poor mechanical strength, which greatly limit their prolonged use in fixed-bed units for large-scale applications.[13–15]

To solve these challenges, many researchers have developed numerous hosts for immobilization of fine HZO nanoparticles inside a solid host to form composite adsorbents that have a larger porous structure and better mechanical strength.[16] Various host materials, such as anion exchange resins,[14,16–18] quaternary-aminated wheat straw particles,[12] and quaternary-ammonium Chinese reed,[19] have been developed for the immobilization of HZO for phosphate uptake. Among them, resins have been widely explored due to the merits of great mechanical strength, high stability, and tunable structure.[14,18] However, the preparation of commercial resins is complicated, and usually accompanied by production of toxic substances such as nitrobenzene, chloromethyl ether, styrene, and divinylbenzene.[12] Recently, hydrogels with crosslinked three-dimensional polymer network structures have attracted great attention in wastewater treatment due to their high adsorption and regeneration capacities, and reusability for continuous processes.[20] Consequently, it is desirable to embed HZO into hydrogels for efficient sequestration of phosphate from water. Among various polymer matrices, increasing attention has been paid to crosslinked poly(vinyl alcohol) (PVA) hydrogels with good biocompatibility, non-toxicity, high mechanical strength, and low cost.[21] For example, Majidnia and Idris[22] prepared maghemite PVA–alginate beads by embedding maghemite nanoparticles in a PVA and alginate matrix for cesium removal from radioactive wastewater. PVA was employed in the immobilization process due to its elasticity and high strength, and the prepared beads are very strong and durable. Although a strategy for developing PVA as polymer matrices has been established, current efforts have focused on decorating PVA with alginate or chitosan matrices to improve the mechanical properties of hydrogels,[23,24] and there is little work devoted to applying PVA as a satisfactory polymer matrix for *in situ* immobilization of HZO.

In this contribution, we report a new strategy for the selective and efficient sequestration of phosphate from aqueous solution, which relies on composite hydrogel beads resulting from simultaneous *in situ* formation of HZO and cross-linking of PVA chains (HZO-PVA) by a facile one-pot strategy (Scheme 1). Considering that the ammonium modification of composite beads can enhance the stability and uptake capacity,[25,26] triethylenetetramine (TETA), which is cheap and contains a high density of N-containing reactive groups,[27] was subsequently grafted on the surface of HZO-PVA (called as TETA@HZO-PVA) to modulate the surface functionality of the beads (Scheme 2). Particularly, the *in situ* formation of HZO with the simultaneous generation of the host framework provides a possible strategy to improve the accessibility of HZO for phosphate capture, resulting in high metal usage efficiencies.

The objective of this work was to evaluate the potential application of TETA@HZO-PVA for the selective and efficient sequestration of phosphate from synthetic water and real wastewater over a wide range of environmentally relevant conditions. To this end, batch experiments were performed to elucidate the phosphate adsorption isotherms, kinetics, and selective sequestration. Desorption experiments were subsequently performed to evaluate the regeneration and reusability of adsorbents. Characterization of the adsorbents before and after phosphate adsorption was conducted to

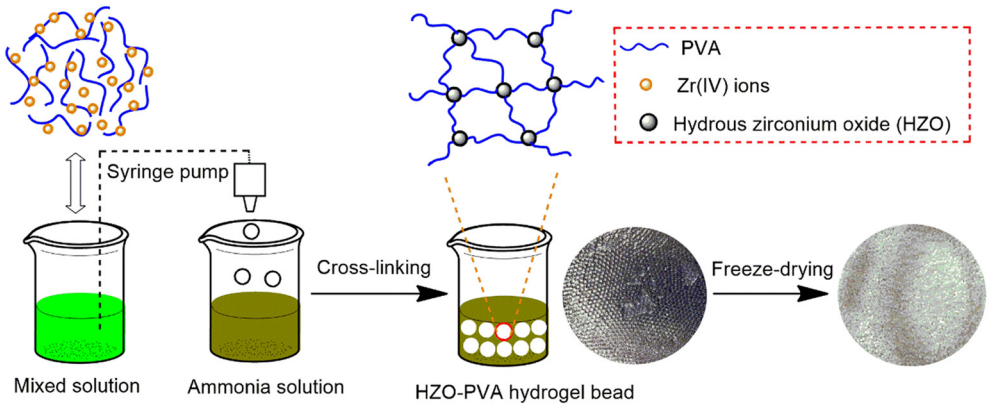

Scheme 1 Schematic illustration for the fabrication of HZO-PVA.

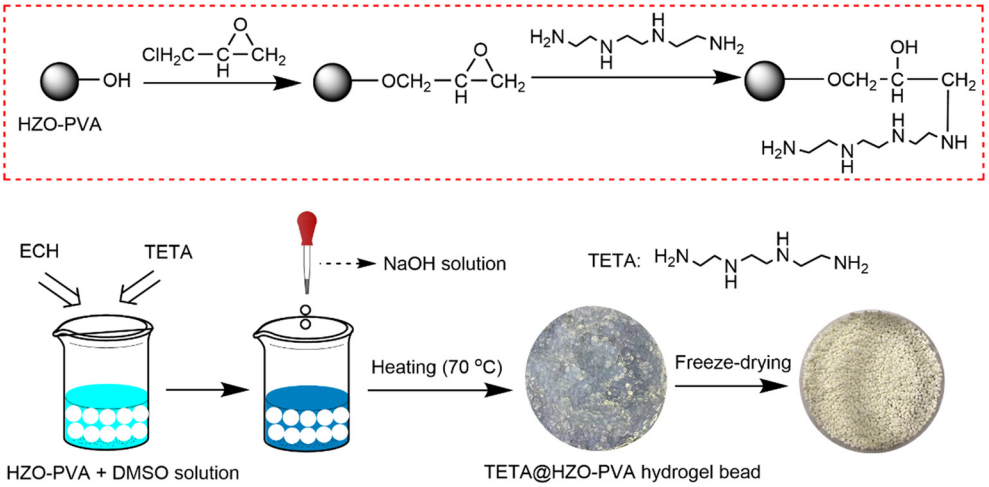

Scheme 2 Schematic illustration for the fabrication of TETA@HZO-PVA.

unveil the sequestration mechanisms. Ultimately, fixed-bed column experiments were designed by feeding with a synthetic solution and real wastewater to evaluate the applicability in effluent treatment. The results gained from this work provided useful information for expanding the scope of application of the unique class of HZO-impregnated materials for phosphate sequestration in water.

2. Materials and methods

2.1. Materials

Poly(vinyl alcohol) (PVA) (M_w = ~145 kDa), zirconium oxychloride octahydrate ($ZrOCl_2{\cdot}8H_2O$, 98%), dimethyl sulfoxide (DMSO, >99%), and epichlorohydrin (ECH, AR) were purchased from Aladdin (Shanghai, China). Triethylenetetramine (TETA) was of analytical grade and obtained from Damao Chemcial Reagent Factory (Tianjin, China). All other reagents were of analytical grade, and were purchased from Shanghai Experiment Reagent Co., Ltd., China. All solutions throughout this study were prepared with deionized (DI) water.

2.2. Preparation of HZO-PVA and TETA@HZO-PVA beads

The facile one-pot fabrication route of HZO-PVA is schematically shown in Scheme 1. About 3 g of PVA was dissolved in 50 mL of DI water with continuous magnetic stirring until complete dissolution. Then, an appropriate amount of $ZrOCl_2{\cdot}8H_2O$ (12.5 mmol) was added into the aqueous solution of PVA to form a homogeneous mixture. The mixture was injected into a 28 wt% ammonia solution using a syringe pump (NE-1000, New Era Pump Systems Inc., USA) that had a 2 mL injector with a 30G steel needle. As soon as the mixture of PVA and zirconium salts made contact with the ammonia solution, HZO-PVA hydrogel beads were formed immediately based on the simultaneous *in situ* formation of HZO and cross-linking of PVA chains. Herein, the *in situ* formed HZO may act as a crosslinker to gelate PVA chains because of strong hydrogen bonding between HZO and hydroxyl groups of PVA chains while the crosslinked PVA could act as a stabilizer to inhibit aggregation or further growth of the *in situ* formed HZO nanoparticles.[21] The obtained HZO-PVA beads were subsequently repeatedly washed with DI water until the solution reached neutral pH, and then freeze-dried before use.

The surface functionalities of HZO-PVA were modified by a facile crosslinking reaction between ECH, amino groups of TETA, and hydroxyl groups of PVA (Scheme 2). Firstly, the as-prepared HZO-PVA beads before freeze-drying were immersed in 100 mL of DMSO solution with adequate mixing, which contained 10 mL TETA and 10 mL ECH. Then, 4 mL of NaOH solution (12.5 mol L^{-1}) was slowly dripped into the mixture at 70 °C with stirring for 10 h to obtain TETA@HZO-PVA beads. Herein, ECH was used to crosslink TETA and PVA in the alkaline solution.[28] The epoxy group in ECH was connected to the crosslinked PVA through the reaction of the hydroxyl groups with ECH. The crosslinked PVA bearing epoxy groups could react with TETA when the temperature and alkali were appropriate to obtain the crosslinked PVA bearing amino groups. Finally, the obtained TETA@HZO-PVA beads were freeze-dried and stored before any use. The magnified photographs of freeze-dried HZO-PVA and TETA@HZO-PVA are shown in Fig. S1.† Compared with that of HZO-PVA, the color of TETA@HZO-PVA changes significantly (Fig. S1†), which may support the amine grafting process of HZO-PVA.

2.3. Batch experiments

All batch experiments were conducted in triplicate in 100 mL centrifuge tubes that were wrapped in aluminum foil at room temperature. Adsorption isotherms were collected by adding 20 mg of freeze-dried adsorbent beads (HZO-PVA or TETA@HZO-PVA) to a centrifuge tube containing 80 mL phosphate solution at initial phosphate concentrations of 5–50 mg L^{-1} on a shaker at a speed of 150 rpm at pH 5.5 ± 0.1 for 24 h. Adsorption kinetics were measured at an initial phosphate concentration of 10 mg L^{-1} and natural pH (5.5 ±

0.1) by monitoring the decrease in the concentration of phosphate at specific time intervals. The phosphate solutions were prepared with KH_2PO_4, and the solution pH was adjusted with a dilute HCl/NaOH solution. The effect of solution pH on adsorption was determined by adjusting the initial pH values from 2 to 10 at an initial phosphate concentration of 10 mg L^{-1}. The effects of competitive anions such as Cl^-, NO_3^-, SO_4^{2-}, and HCO_3^- as well as dissolved organic matter (DOM) like humic acid (HA) and fulvic acid (FA) on adsorption were evaluated by adding the required amounts of NaCl, $NaNO_3$, Na_2SO_4, $NaHCO_3$, HA, and FA to phosphate solutions (5 mg L^{-1}) at natural pH 5.9 ± 0.1.

Desorption and regeneration experiments were conducted and repeated five times. After complete adsorption at an initial phosphate concentration of 5 mg L^{-1} and natural pH, the saturated adsorbent beads were recovered by simple filtration followed by mixing with 0.25 mol L^{-1} NaOH solution on an oscillator for 3 h. Then, the beads were transferred into 0.1 mol L^{-1} HCl solution for 3 h for regeneration and subsequently washed with DI water before the next adsorption. The measurements of adsorption performance and desorption efficiency, adsorption kinetics models, and adsorption isotherm models are described in the ESI.†

2.4. Fixed-bed column experiments

Fixed-bed column adsorption trials were performed to evaluate the real application capacity. A commercial glass tube was used to imitate a column with an inner diameter of 1.5 cm as reported in the literature.[25,29,30] The influent was upward pumped through the column packed with 16 cm^3 wet TETA@HZO-PVA beads at a flow rate of 5 mL min^{-1} using a peristaltic pump (Chuangrui Pump, BT100M, China), and the corresponding empty bed contact time (EBCT) was 3.2 min. The column experiments were performed with a synthetic solution and real municipal wastewater for a comparative study. The real wastewater sample taken from a wastewater treatment plant in Guangzhou City was filtered using a 0.45 μm membrane filter to remove suspended impurities, and then introduced into the column without any pH alteration. The main composition of the sewage was determined as follows: pH 7.65, electrical conductivity 7.82 mS cm^{-1}, chemical oxygen demand (COD) 48.00 mg L^{-1}, orthophosphate (PO_4-P) 3.08 mg L^{-1} and ammonium (NH_4-N) 29.65 mg L^{-1}. The synthetic sample was a 3.08 mg L^{-1} phosphate-containing solution made by dissolving an appropriate amount of KH_2PO_4. The concentration of phosphate from the effluent after passing through the column was determined at regular time intervals.

After column adsorption, the exhausted adsorbent beads were washed with DI water for 0.5 h and then *in situ* regenerated by pumping 0.25 mol L^{-1} NaOH solution at a flow rate of 5 mL min^{-1}. The eluted effluent was collected at regular time intervals and evaluated for effluent phosphate concentration. The determination of column adsorption performance and column adsorption models are described in the ESI.†

2.5. Analysis and characterization

The phosphate concentration was measured by the ammonium molybdate spectrophotometric method with a detection limit of 0.01 mg L^{-1}.[29] The morphologies of HZO-PVA and TETA@HZO-PVA were observed by scanning electron microscopy (SEM) (JSM-7001F, JEOL, Japan). The functional groups of HZO-PVA and TETA@HZO-PVA were determined by Fourier transform infrared spectroscopy (FT-IR) (Tensor 27, Bruker, Germany). The crystalline structures of HZO-PVA and TETA@HZO-PVA were recorded using X-ray diffraction measurements (XRD, Raguku Ultima IV, Japan). Thermogravimetric analysis (TGA) was conducted on a thermogravimetry analyzer (TGA4000, PerkinElmer, USA) at a heating rate of 10 °C min^{-1} in a N_2 flow. The analysis of surface electronic states was performed by X-ray photoelectron spectroscopy (XPS) (250XI, Thermo ESCALAB, USA), and all the binding energies were calibrated using the C 1s peak (284.8 eV).[25] The values of pH at the point of zero charge (pH_{pzc}) for HZO-PVA and TETA@HZO-PVA were determined by the pH drift method.[31–33] For this purpose, 80 mL of 0.1 mol L^{-1} NaCl solution was placed in a 100 mL centrifuge tube, and N_2 was bubbled through the solution to stabilize the pH by preventing the dissolution of CO_2. The pH was then adjusted to successive initial values from 2 to 12 with 1 mol L^{-1} HCl or NaOH solution, and 0.02 g of the as-prepared beads (HZO-PVA or TETA@HZO-PVA) was added into the solution. The final pH value was recorded after 24 h continuous stirring at ambient temperature and plotted against the initial pH. The pH at which the curve crosses the line pH(final) = pH(initial) is taken as the pH_{pzc} of the as-prepared beads. In order to evaluate the stability of HZO-PVA and TETA@HZO-PVA in water at different pH values, the Zr leaching and polymer leaching from the beads were measured by immersing 20 mg beads in 80 mL phosphate solution (10 mg L^{-1}) at different pH values (2–10) at 150 rpm for 48 h. The result of polymer leaching was examined using a total organic carbon (TOC) analyzer (liquid TOC II, Elementar, Germany) with a detection limit of 0.2 mg L^{-1}, and the concentration of Zr leached into solution was determined by inductively coupled plasma-mass spectrometry (ICP-MS) (NexION 300, PerkinElmer, USA).

3. Results and discussion

3.1. Characterization of the as-prepared adsorbent beads

The SEM images show that the freeze-dried HZO-PVA and TETA@HZO-PVA beads exhibited a spherical shape with a moon-like structure (Fig. 1a and c). Compared to HZO-PVA, the surface of TETA@HZO-PVA was grafted with a layer of TETA that created a higher degree of surface roughness, demonstrating the successful attachment of TETA (Fig. 1b and d). Such a rougher surface of the adsorbent bead would provide more adsorption sites for phosphate.[34] The

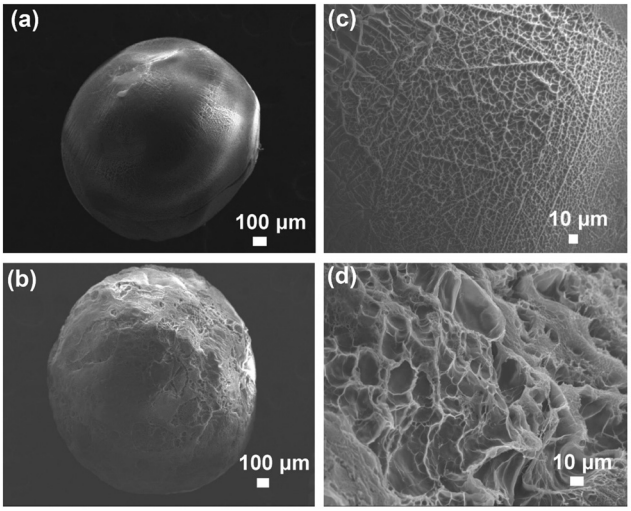

Fig. 1 SEM images of (a) whole freeze-dried HZO-PVA, (b) whole freeze-dried TETA@HZO-PVA, (c) surface structure of freeze-dried HZO-PVA, and (d) surface structure of freeze-dried TETA@HZO-PVA.

crystalline structures of HZO-PVA and TETA@HZO-PVA were illustrated by XRD patterns as depicted in Fig. S2.† The characteristic peak at 2θ = 19.6° was assigned to the semicrystalline feature of the PVA matrix.[21] However, no crystalline peaks were detected for HZO nanoparticles in the XRD patterns of HZO-PVA and TETA@HZO-PVA, indicating that the HZO nanoparticles are mostly amorphous. Similar results were also reported by others.[12,35] To investigate the thermal stability of the adsorbent beads, TGA measurement was performed as depicted in Fig. S3.† The TGA curves show that PVA was almost completely decomposed when the temperature exceeds 500 °C, and the residue weight was 5.3 wt%. However, the organic components of HZO-PVA and TETA@HZO-PVA were completely decomposed until about 700 °C, and their residue weights were 38.4 wt% and 28.0 wt%, respectively. These results indicate that HZO-PVA and TETA@HZO-PVA possessed a much higher thermal stability than the corresponding polymer, which is primarily attributed to the presence of the cross-linked structure and HZO components.[21]

3.2. Batch sequestration performance

Adsorption kinetics measurements were firstly performed to determine the sequestration rate for HZO-PVA and TETA@HZO-PVA at an initial phosphate concentration of 10 mg L^{-1} and natural pH. Fig. 2a shows that the adsorption increased rapidly at the early stage and then gradually reached equilibrium within 24 h. TETA@HZO-PVA exhibited a better adsorption capacity compared to HZO-PVA (24.70 *vs.* 9.05 mg g^{-1}) (Table S1†), which is largely due to the surface amino functional groups that provided more adsorption sites for phosphate.[25,36] The pseudo-second-order (PSO) kinetic

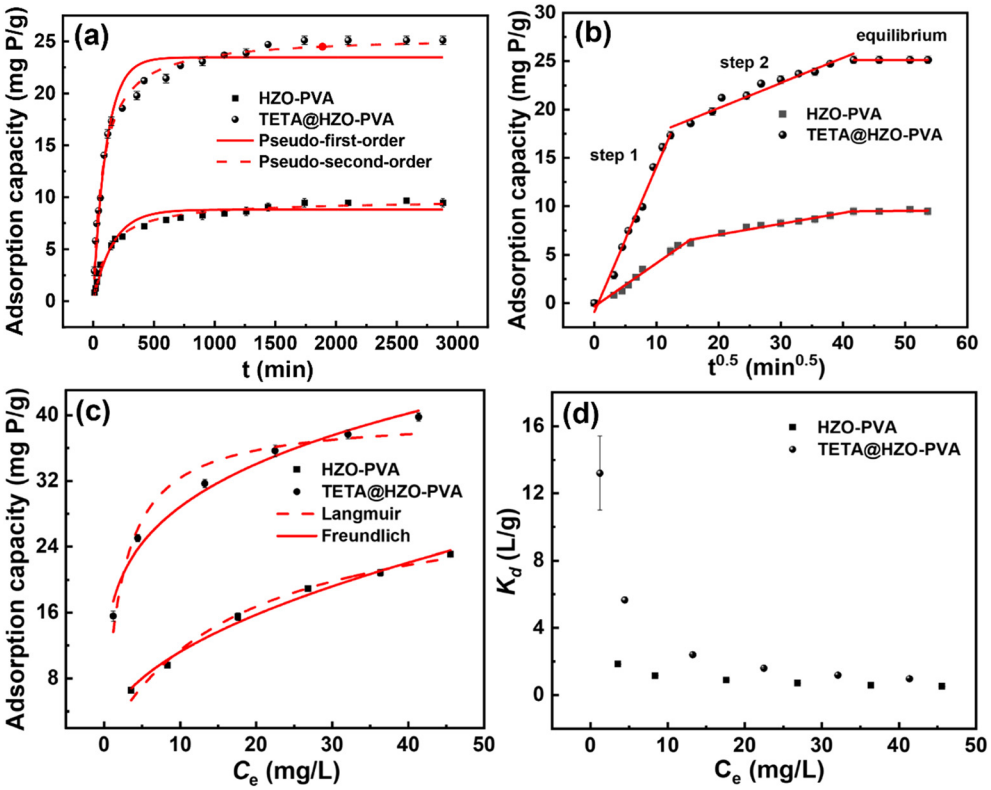

Fig. 2 (a) Kinetic curves fitted by the pseudo-first-order and pseudo-second-order models. (b) Intraparticle diffusion modeling curves. (c) Isotherms by Langmuir and Freundlich fitting. (d) Distribution coefficients (K_d) calculated based on isotherm data.

model showed higher correlation coefficients ($R^2 > 0.99$) than the pseudo-first-order (PFO) kinetic model. The equilibrium adsorption capacity calculated from the PSO model agreed well with the experimental data for HZO-PVA and TETA@HZO-PVA (9.74 *vs.* 9.05 mg P per g; 24.70 *vs.* 25.54 mg P per g) (Table S1†). These findings suggest that the PSO kinetic model, based on the assumption that the rate-limiting step may be chemical sorption or chemisorption involving valence forces through sharing or exchange of electrons between the adsorbent and adsorbate, provided a better correlation of the data.[37] The empirical equation generally known as the Elovich equation has been extensively applied to chemisorption data.[38,39] The nonlinear fitting results by the Elovich kinetic model are shown in Fig. S6 and Table S1.† It was apparent that the R^2 values calculated from the Elovich kinetic model for HZO-PVA and TETA@HZO-PVA were 0.979 and 0.958, respectively. The good fitting by the Elovich kinetic model may suggest that the chemisorption took place between phosphate and the prepared beads (HZO-PVA and TETA@HZO-PVA).[40]

To further evaluate the rate-limiting step of the phosphate adsorption process, the Weber–Morris intraparticle diffusion model was employed. Fig. 2b shows that the plots of q_t *versus* $t^{0.5}$ present multilinearity, indicating that a multistep process controls the overall rate of phosphate adsorption.[17] The first linear region has a steeper slope which refers to the diffusion of phosphate from solution to the surface of adsorbent beads, where surface or film diffusion is the rate-controlling step. The second linear region has a lower slope which refers to the diffusion of phosphate within the adsorbent beads, where intraparticle diffusion is considered as the rate-limiting step. This can be evidenced by the much lower values of k_{2d} with respect to those of k_{1d} for the first stage (Table S2†), which is due to the increased diffusion resistance when phosphate ions diffuse into the pores of adsorbent beads.[12,17] The third linear region represents the final equilibrium stage, where the rates of adsorption and desorption remain equivalent due to the low concentration of phosphate and the saturation of adsorption sites.

To evaluate the sequestration capacities for HZO-PVA and TETA@HZO-PVA, the adsorption isotherm measurements were conducted at different initial phosphate concentrations (5–50 mg L^{-1}). The Langmuir model and Freundlich model were employed to describe the phosphate adsorption isotherms on HZO-PVA and TETA@HZO-PVA (Fig. 2c). The fitting parameters are summarized in Table S1.† The Freundlich model better described the adsorption processes of phosphate onto both HZO-PVA and TETA@HZO-PVA than the Langmuir model as indicated by the higher correlation coefficients (R^2) (Table S1†), suggesting that the adsorption sites on the composite beads were heterogeneous.[41] The Freundlich constant K_L value of TETA@HZO-PVA was about 4.6 times higher than that of HZO-PVA, indicating that TETA@HZO-PVA exhibited a stronger affinity for phosphate than HZO-PVA.[14] To further quantify the phosphate affinity of adsorbent beads, the distribution coefficient K_d (L g^{-1}) was calculated (as described in eqn (S10)†) (Fig. 2d). As expected, TETA@HZO-PVA exhibited superior K_d values, confirming the exceptional affinity towards phosphate.[14] The maximum adsorption density of phosphate of TETA@HZO-PVA (39.87 mg P per g), estimated from the Langmuir model, was higher than that of HZO-PVA (31.23 mg P per g). Enhanced phosphate sequestration can be intimately linked with the surface functionalized amino groups grafted on the surface of TETA@HZO-PVA which elevated the phosphate uptake; the detailed mechanism was elucidated by XPS as discussed below. The maximum adsorption density of phosphate of TETA@HZO-PVA was higher compared to those of previous adsorbents such as HZO immobilized in quaternary-aminated wheat straw (Ws-N-Zr) (31.9 mg P per g at pH 6.0 and 298 K),[12] zirconium loaded okara (15.1 mg P per g at natural pH and 318 K),[42] and zirconium-modified activated sludge (27.6 mg P per g at pH 4.0 and 298 K).[43]

Considering that the surface hydroxyl groups of HZO and amino groups in the functionalized adsorbent beads are pH-dependent in aqueous solution,[19] we thus further evaluated the phosphate uptake as a function of initial pH from 2.0 to 10.0 (Fig. 3a). The adsorption capacities decreased from 34.4 mg P per g to 1.84 mg P per g for HZO-PVA and from 40.0 mg P per g to 12.9 mg P per g for TETA@HZO-PVA as the solution pH increased from 2 to 10. Similar trends could be observed in previous studies.[26,44,45] Obviously, high adsorption performances were obtained under acidic conditions for both adsorbents, which could be interpreted as follows:[45] (i) the surface of adsorbents was positively charged at low pH, enhancing the affinity toward the negatively charged $HPO_4^{2-}/H_2PO_4^-$ species; (ii) though the dominant adsorption process was ligand exchange, a higher positive charge can be generated since $-NH_2$ can be protonated to form $-NH_3^+$; and (iii) increasing the pH leads to a change in the phosphate species from $H_2PO_4^-$ to HPO_4^{2-} to PO_4^{3-} with increasingly lower reactivity. Under highly acidic conditions (*i.e.*, pH = 2–3), $H_2PO_4^-$ was the major phosphate species (Fig. S4†) with a small amount of H_3PO_4 that cannot be effectively adsorbed onto TETA@HZO-PVA. At the same time, when the pH was below pH_{pzc} (≈6.9, see Fig. S5†), the surface hydroxyl groups of HZO and amino groups in TETA@HZO-PVA could be protonated. The positive charge favored the interaction with the major species $H_2PO_4^-$ through strong electrostatic attraction at lower pH. Besides, the obviously positive ΔpH (= final pH − initial pH) (Fig. 3b) showed that ligand exchange may contribute to the increased phosphate adsorption onto TETA@HZO-PVA by forming an inner-sphere complex.[46,47] The obviously positive ΔpH showed that the final pH was higher than the initial pH, illustrating the increase of the hydroxide amount in solution after phosphate adsorption. This phenomenon might be interpreted as the release of hydroxide from the ligand exchange between phosphate and hydroxyl groups from the adsorbents.[48] Moreover, at lower pH, $-OH_2^+$ (positively charged surface hydroxyl group) can be more easily displaced from the metal binding sites than the hydroxyl groups,

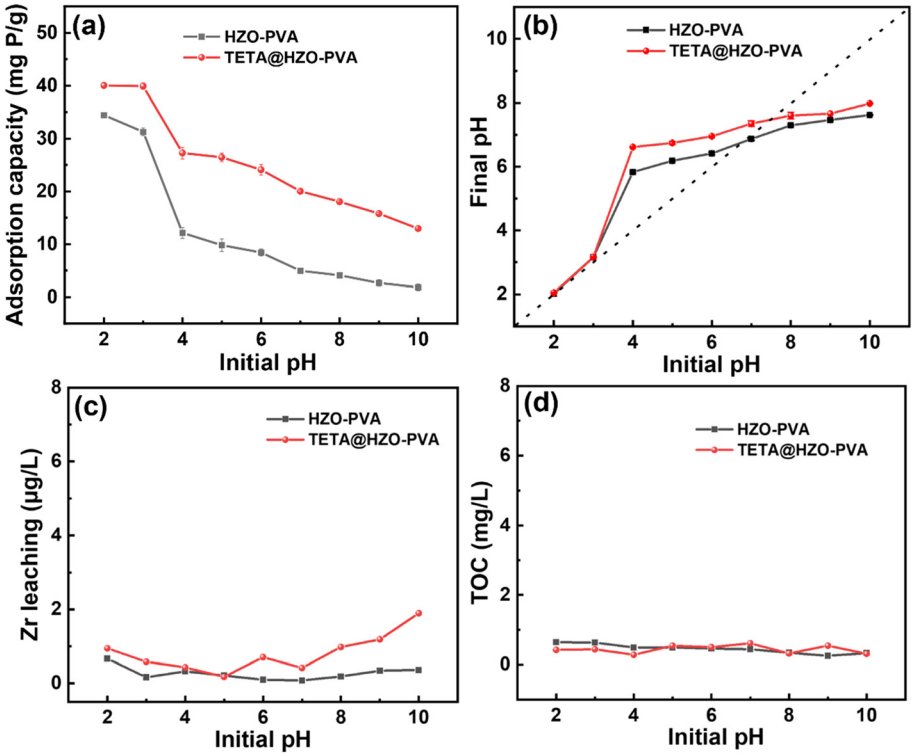

Fig. 3 (a) Effect of initial pH on phosphate adsorption, (b) final pH variation of the solution, (c) pH-dependent Zr leaching, and (d) polymer leaching from HZO-PVA and TETA@HZO-PVA as determined from total organic carbon.

favoring the release of more hydroxide groups of the adsorbents into solution during the ligand exchange process.[48] Similar results can be observed in previous studies.[46–50] When the pH > 3.0, the electrostatic attraction was weakened and in contrast ligand exchange would dominate the adsorption process at higher pH.[19] However, under alkaline conditions (pH = 7–10), the predominant species was HPO_4^{2-} (Fig. S4†), and the surface of TETA@HZO-PVA was deprotonated and negatively charged. Strong electrostatic repulsion between the negatively charged $Zr–O^-$ and HPO_4^{2-} occurred, which simultaneously weakened the ligand exchange process, resulting in a sharp reduction in adsorption capacity. The decreased ΔpH (Fig. 3b) indicated that the ligand exchange process became weaker. Meanwhile, the Lewis acidic properties of Zr favored its high affinity with the oxygen anions in phosphate to form an inner-sphere complex through the Lewis acid–base interaction, which governed the comparatively stable adsorption capacities at high pH values.[46] Consistent with the results of isotherms and kinetics, the adsorption capacity of TETA@HZO-PVA was always higher compared to that of HZO-PVA under the same pH conditions, which may be ascribed to the presence of more active sites (*e.g.*, amino groups) and the enhancement of surface properties due to the surface functionalities of TETA. The pK_a values of TETA were reported to be 9.2 and 9.92, characterized by two primary amines and two secondary ones.[51] Compared to that of the pristine HZO-PVA, the zeta potentials of modified ones with TETA were expected to lean more toward positive values.[52] Fig. S5† shows that after TETA modification, the pH_{pzc} of HZO-PVA was increased from 6.3 to 6.9, confirming that this modification enhances protonation and also suggests that TETA was successfully grafted onto HZO-PVA.

Next, we evaluated the chemical stability of adsorbent beads during the phosphate adsorption under different pH conditions (Fig. 3c and d). After being immersed in the working solution for 48 h, less than 2 μg L^{-1} Zr (or 0.008 mg Zr per g) was leached into the solution over the whole pH range for both HZO-PVA and TETA@HZO-PVA (Fig. 3c). Further, the amount of TOC leakage from the two materials was below 1 mg L^{-1} after 48 h of immersion across all pH conditions tested. These observations indicate that the crosslinked PVA host enhanced the stability of the immobilized HZO nanoparticles over a wide range of pH. Compared with zirconium hydroxide encapsulated in quaternized cellulose (QC-Zr) with a leakage of Zr of 0.59 mg Zr per g at pH < 3 and TOC of >200 mg L^{-1} at pH > 8 after being shaken for 24 h,[53] the as-prepared HZO-PVA and TETA@HZO-PVA in this study are very advantageous with preferable chemical stability during the phosphate adsorption processes.

In practical applications, many common anions such as Cl^-, NO_3^-, SO_4^{2-}, and HCO_3^- as well as DOM (*e.g.*, humic acid and fulvic acid) can co-exist in phosphate contaminated waters. It is thus of particular importance to explore the selective performance of TETA@HZO-PVA for phosphate

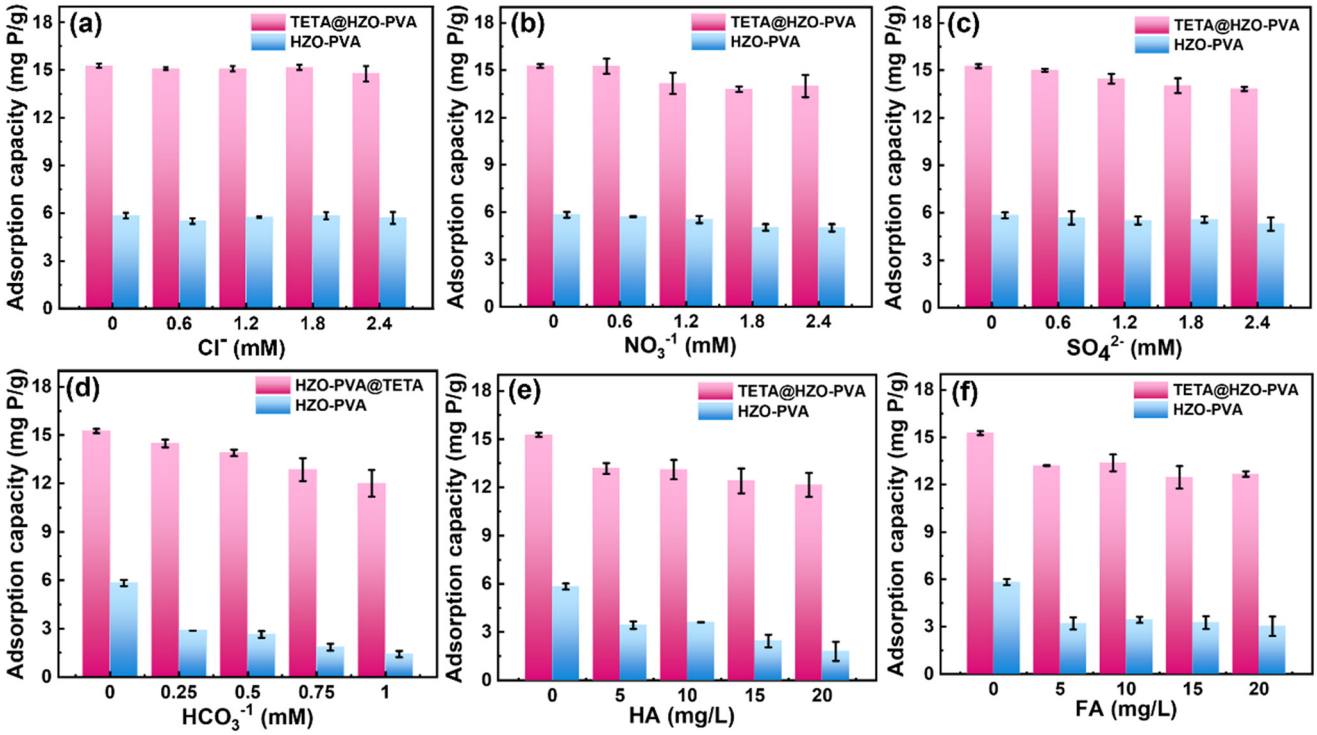

Fig. 4 Effect of competing anions and DOC on phosphate adsorption by HZO-PVA and TETA@HZO-PVA: (a) Cl^-, (b) NO_3^-, (c) SO_4^{2-}, (d) HCO_3^-, (e) humic acid (HA), and (f) fulvic acid (FA).

sequestration. As depicted in Fig. 4a, Cl^- had almost no influence on the adsorption capacity with a concentration of up to 2.4 mM. Also, NO_3^- and SO_4^{2-} had a negligible or little impact on phosphate adsorption even at a relatively high concentration. While HCO_3^- is typically recognized to be a competitor for affinity sites with phosphate on adsorbent beads,[41] TETA@HZO-PVA retained a high phosphate sequestration efficiency (~79%) even in the presence of 1 mM HCO_3^-. Prior studies reported that humic acid and fulvic acid can compete with phosphate for the active sites of metal-containing adsorbents through the formation of complexes with metal oxides.[53] It is interesting that even in the presence of 20 mg L^{-1} humic acid and fulvic acid, TETA@HZO-PVA still retained an ~80% phosphate uptake. Such remarkable selectivity and anti-interference ability of TETA@HZO-PVA may be ascribed to the presence of surface ammonium groups from TETA which prevents the coexisting ions from approaching the active sites of TETA@HZO-PVA.[36] Taken together, the as-prepared TETA@HZO-PVA is potentially expected to exhibit removal selectivity for phosphate sequestration in practical wastewater treatment.

3.3. Mechanism for phosphate sequestration

Phosphate adsorption can be usually accomplished by its nonspecific interactions (*e.g.*, electrostatic attraction or outer-sphere complexation) or specific interactions (*e.g.*, inner-sphere complexation) with the functional groups of the adsorbent.[54] The validity of the three main mechanisms for phosphate sequestration (electrostatic attraction, ligand exchange, and Lewis acid–base interactions) is supported by the comparison of phosphate sequestration under different pH conditions. To explore the underlying mechanisms of phosphate adsorption onto HZO-PVA and TETA@HZO-PVA, the spectroscopic techniques FTIR and XPS were performed. Fig. 5 shows the FTIR spectra of HZO-PVA and TETA@HZO-PVA before and after phosphate adsorption. The main characteristic peaks for virgin HZO-PVA (Fig. 5a) could be observed as follows: 3400 cm^{-1} (O–H stretching vibration), 2938 cm^{-1} (C–H stretching from alkyl groups), and 1100 cm^{-1} (C–O vibration in PVA).[55,56] The O–H bending vibration in

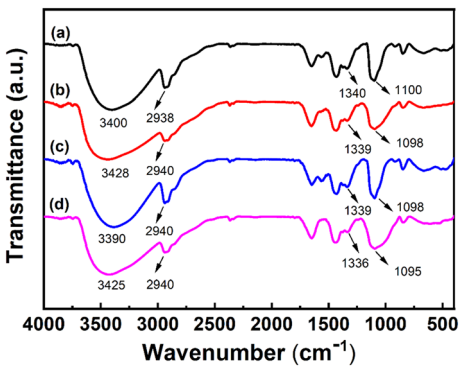

Fig. 5 FTIR spectra of HZO-PVA (a) before adsorption and (b) after adsorption. FTIR spectra of TETA@HZO-PVA (c) before adsorption and (d) after adsorption.

HZO-PVA was observed at 1340 cm^{-1}, indicating the presence of surface hydroxyl groups on the composite (mostly Zr–OH).[12] However, after adsorption, the O–H bending vibration peak of surface hydroxyl (1340 cm^{-1}) weakened. The P–O stretching region usually gave a band at 1000–1100 cm^{-1}.[57] A broader peak at ~1098 cm^{-1} after adsorption was observed, which could be ascribed to the overlap of initial C–O vibration in PVA and characteristic P–O stretching at the same region.[58] These changes indicated the substitution of surface hydroxyl groups by phosphate species, revealing the formation of an inner-sphere complex between phosphate and the *in situ* formed HZO. The spectra of TETA@HZO-PVA before and after phosphate adsorption (Fig. 5c and d) showed similar patterns, implying the successful phosphate capture due to the formation of an inner-sphere complex. Comparison of the spectrum of virgin HZO-PVA and TETA@HZO-PVA clearly showed that the peak of –OH stretching vibration shifted from 3400 cm^{-1} to 3390 cm^{-1}, possibly due to the overlap of O–H and N–H stretching vibration.[59] This further indicates that TETA was successfully grafted on the surface of HZO-PVA *via* a facile chemical crosslinking reaction.[59] Besides, a notable shift of O–H and N–H stretching vibration from 3390 cm^{-1} to 3425 cm^{-1} after phosphate adsorption was detected. This suggests that the reactive amino groups of TETA might participate in the adsorption process.

The surface hydroxyl and amino group interactions with phosphate were further investigated by XPS. The spectra were fitted using XPSPEAK41 software, and the corresponding data are summarized in Tables S3 and S4.† Fig. S7a† shows the appearance of main peaks such as C 1s, O 1s, Zr 3d, and P 2p in the total survey spectra of HZO-PVA (before and after adsorption). The emergence of P 2p further confirmed that phosphate was adsorbed on HZO-PVA. Compared with the P 2p spectrum of purified KH_2PO_4 centered at ~134.0 eV,[60] a remarkable shift in the P 2p spectrum to a lower binding energy of 133.57 eV was detected for HZO-PVA (Fig. S7d†). This indicates the formation of chemical bonds between phosphate and HZO-PVA through the coordination of the oxygen anions of phosphate with the unoccupied orbitals at the Zr(IV) sites *via* Lewis acid–base interactions.[41] Fig. S7b and e† illustrate the O 1s spectra of HZO-PVA before and after phosphate adsorption. The O 1s peak could be well fitted with three overlapped O 1s peaks, including hydroxyl groups (–OH), oxide oxygen (O^{2-}), and carbon oxygen (C–O) originating from the host.[12] It is clear that the –OH percentage in HZO-PVA decreased from 20.9% to 17.7% after phosphate adsorption, indicating the replacement of –OH groups by phosphate species during the adsorption process.[12,61] This is consistent with the FTIR analysis. Fig. S7c and f† display that the double peaks assigned to Zr $3d_{3/2}$ and Zr $3d_{5/2}$ in HZO-PVA shifted from 184.77 eV and 182.39 eV to higher binding energies of 184.98 eV and 182.60 eV, respectively, after phosphate adsorption, illustrating the possible electron transfer in the valence band of Zr 3d and the formation of a Zr–O–P inner-sphere complex.[41] Similar

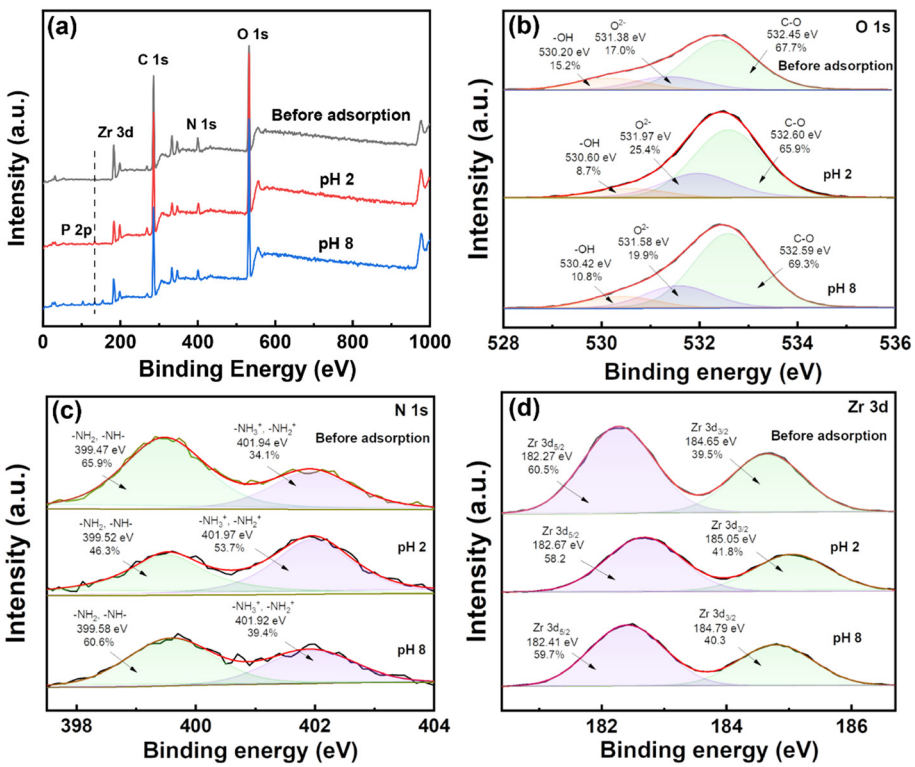

Fig. 6 XPS analysis of TETA@HZO-PVA before and after phosphate adsorption under different pH conditions: (a) wide-scan spectra; (b) O 1s; (c) N 1s; (d) Zr 3d.

results can be observed in previous studies.[41,62] Therefore, both the FTIR and XPS analyses confirmed that the replacement of surface hydroxyl groups by phosphate species played an important role in the adsorption process of phosphate onto HZO-PVA, and revealed the formation of a Zr–O–P inner-sphere complex between phosphate and the *in situ* generated HZO.

The XPS wide scan spectra of TETA@HZO-PVA before and after phosphate adsorption under different pH conditions are shown in Fig. 6a. The biggest difference between the total survey spectra of HZO-PVA and TETA@HZO-PVA was the appearance of N 1s, which demonstrated the successful introduction of TETA. Fig. S8† displays the notable downshift of the P 2p peak after the adsorption process at both pH 2 and 8 in comparison with the baseline of KH_2PO_4 (~134.0 eV), confirming the formation of strong Zr–O–P chemical bonds.[41] Similar results were also observed in the high-resolution spectra of O 1s and Zr 3d for TETA@HZO-PVA before and after phosphate adsorption at both pH 2 and 8. It should be pointed out that the proportion of the –OH group was calculated as 15.2% for the original TETA@HZO-PVA, with that determined as 8.7% and 10.8% for phosphate adsorbed TETA@HZO-PVA at pH 2 and 8 respectively (Fig. 6b). The remarkable decreased proportion of the –OH group indicated a higher utilization ratio of –OH group for phosphate adsorption onto TETA@HZO-PVA when contrasted with the –OH percentage in HZO-PVA after phosphate adsorption. This is likely due to the fact that the amino groups improved the mass transfer rate of phosphate.[36] By contrast, the reduction of –OH content at pH 8 was less than that at pH 2, confirming that the –OH groups played a crucial role in the phosphate adsorption process under acidic conditions.[39] Moreover, the N 1s spectra of TETA@HZO-PVA before and after phosphate adsorption are given in Fig. 6c. The two peaks in the N 1s spectrum of virgin TETA@HZO-PVA located at 399.47 eV and 401.94 eV were assigned to neutral N ($-NH_2$ and/or –NH–) and positively charged N ($-NH_3^+$and/or $-NH_2^+$).[63] After adsorption, the area ratio for the peak related to $-NH_3^+$ and/or $-NH_2^+$ was increased from 34.1% to 53.7% at pH 2, while it was increased from 34.1% to 39.4% at pH 8. The remarkable increase of $-NH_3^+$ and/or $-NH_2^+$ suggested that more $-NH_3^+$ and/or $-NH_2^+$ groups were formed during the adsorption process at pH 2, and the positive potentials of TETA@HZO-PVA caused by amino protonation could be used for the adsorption of phosphate anions.[26]

Taken as a whole, the high adsorption capacity of phosphate onto TETA@HZO-PVA is caused by the combined mechanisms of electrostatic attraction, ligand exchange, and Lewis acid–base interactions, which jointly promoted phosphate sequestration but played different roles under different pH conditions. The surface functionalized TETA could improve the utilization ratio of –OH groups and facilitate the positive potential, resulting in enhanced phosphate sequestration. The possible phosphate sequestration mechanisms are proposed in Scheme 3. Under acidic conditions (pH = 3–6), $H_2PO_4^-$ was the major phosphate species, and the surface of TETA@HZO-PVA was protonated and positively charged ($pH_{pzc} \approx 6.9$); thus, the electrostatic attraction between active sites and $H_2PO_4^-$ contributed to the sequestration of phosphate. Besides, the obviously positive ΔpH of the solution pH indicated that ligand exchange also had the main contribution for phosphate sequestration. In fact, when the pH was below pH_{pzc}, the surface hydroxyl groups of HZO could be protonated as follows: $Zr–OH + H^+ \rightarrow Zr–OH_2^+$.[64] The $–OH_2^+$ species (positively charged surface hydroxyl groups) were easier to displace from the metal binding sites than the hydroxyl groups,[46,47] which facilitated the ligand exchange process and can be expressed as follows: $Zr–OH_2^+ + H_2PO_4^- \rightarrow Zr–OH_2^+ \cdot H_2PO_4^- \rightarrow Zr–O–P(OH)_3^+ + OH^-$.[49] Furthermore, the ratio of surface hydroxyl groups before and after phosphate sequestration dropped from 14.7% to 8.9%, which suggested the substitution of hydroxyl groups by phosphate species through ligand exchange, revealing the formation of an inner-sphere complex between phosphate and the impregnated HZO. Under alkaline conditions, the predominant species was HPO_4^{2-}, and the surface of TETA@HZO-PVA was deprotonated

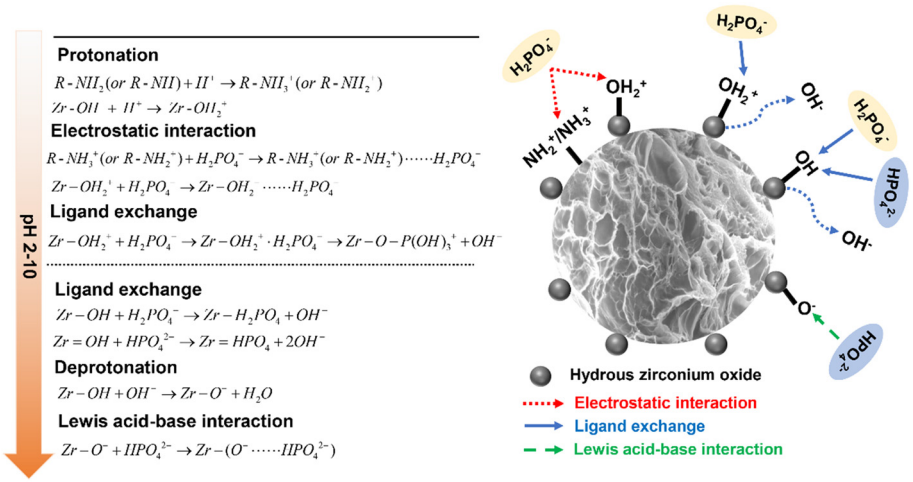

Scheme 3 Possible phosphate sequestration mechanism of TETA@HZO-PVA.

and negatively charged. Thus, the effect of electrostatic attraction became negligible and simultaneously, the ligand exchange mechanism became weaker due to deprotonation on the surface of TETA@HZO-PVA, resulting in the decreased ΔpH of the solution pH.[46] Therefore, the phosphate sequestration onto TETA@HZO-PVA under alkaline conditions could be mainly related to the Lewis acid–base interaction mechanism in which Zr active sites react with oxygen anions in phosphate to form the Zr–O–P inner-sphere complex.[41] The Lewis acid–base interaction mechanism could dominate the comparatively stable phosphate sequestration onto TETA@HZO-PVA at high pH values.[46]

3.4. Regeneration test

The ability to regenerate and recycle adsorbents is of great importance to afford great advantages in reducing costs and facilitating practical applications.[65] To this end, the possibility of regeneration and reusability of HZO-PVA and TETA@HZO-PVA were evaluated. The decreased adsorption performance observed at pH 10 as shown in Fig. 3a indicated that the adsorbent beads could be regenerated by alkaline treatment. Indeed, the desorption and reusability tests confirmed the acceptable repeated use of the adsorbent beads for phosphate removal and recovery. Fig. 7 shows that a slight decrease in adsorption capacity was observed for both HZO-PVA and TETA@HZO-PVA in successive adsorption–desorption cycles. Significantly, the adsorption capacities of HZO-PVA and TETA@HZO-PVA remained at ~90% of the original phosphate adsorption capacities even after five cycles. The good recyclability makes HZO-PVA and TETA@HZO-PVA technically and economically preferable for practical applications. The slight reduction in adsorption capacity after five cycles may be due to the strong chemical bonding between the preloaded phosphate and adsorbents, resulting in the deactivation of some adsorption sites by irreversible adsorption.[41] More impressively, the preloaded phosphate could be effectively desorbed with a regeneration efficiency >85% and >89% in the five cycles for HZO-PVA and TETA@HZO-PVA, respectively (see Fig. 7). Altogether, HZO-PVA and TETA@HZO-PVA could be employed for preferable phosphate removal and recovery without significant performance reduction during repeated use. It is worth mentioning that the eluent after adsorption cycles could be received as a concentrated phosphate solution, and can be used as a raw material to produce agricultural or industrial products.[41]

3.5. Continuous column adsorption and regeneration

Inspired by the efficient and selective sequestration of phosphate by TETA@HZO-PVA, we then conducted fixed-bed column experiments to gain further insights into the practical applicability potential of TETA@HZO-PVA. Fig. 8a shows the breakthrough curves of phosphorus adsorption on TETA@HZO-PVA by employing real wastewater and a synthetic solution as a feed solution under natural pH conditions. The detailed column parameters are available in Table S5.† Based on the recommended discharge limit (0.5 mg P per L) according to the effluent discharge standard of China (GB18918-2002),[53] the effective treatment volume of TETA@HZO-PVA with the real wastewater and synthetic solution as a feed solution was ~440 and 840 bed volume (BV), respectively. These observations demonstrate that TETA@HZO-PVA was capable of cleaning real wastewater to permissible limits for phosphate. The column equilibrium adsorption capacity (q_e, mg P per g) was higher in the synthetic solution than in real wastewater (27.89 *vs.* 20.13 mg P per g) (Table S5†). This may be explained by the presence of complex chemical composition in real wastewater which decreased the effective adsorption site density towards phosphate. The exhausted TETA@HZO-PVA in the column can be *in situ* regenerated with 0.25 mol L^{-1} NaOH solution at a flow rate of 5 mL min^{-1}. Fig. 8b shows that the laden phosphorus could be effectively extracted by the eluting solution, achieving a high cumulative desorption rate of >95% after 56.25 BV for adsorption trials for both the real wastewater and synthetic solution. The above results suggest that TETA@HZO-PVA can serve as a potential alternative in practice for phosphorus contaminated water.

To further evaluate the dynamic column adsorption system, the Thomas model was adopted, which is widely used

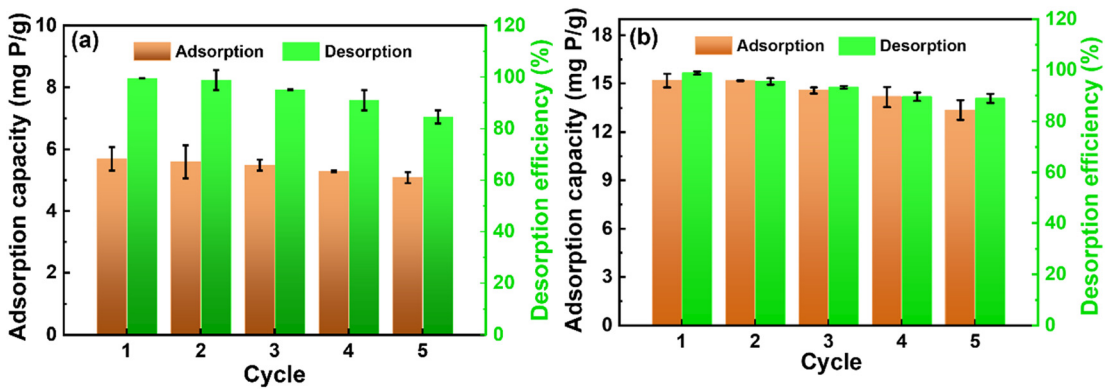

Fig. 7 Effect of recycling times on the adsorption–desorption behaviors of (a) HZO-PVA and (b) TETA@HZO-PVA.

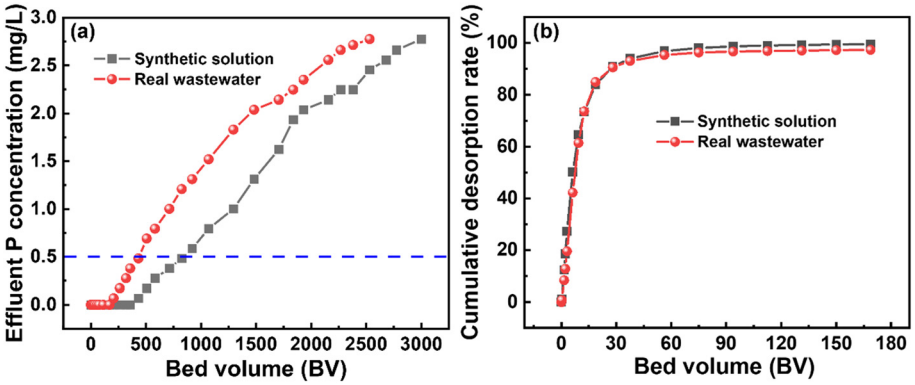

Fig. 8 (a) Breakthrough curves of the fixed-bed column packed with TETA@HZO-PVA by using different feed solutions (adsorbent loading: 16 cm^3, flow rate: 5.0 mL min^{-1}, and influent phosphorus concentration: 3.08 mg L^{-1}). (b) The cumulative desorption curves of saturated columns.

to describe column adsorption data. Fig. S9 and Table S5† show that the dynamic adsorption data in the fixed-bed column can be well described by the Thomas model as indicated by high correlation coefficients ($R^2 > 0.96$). The equilibrium absorption capacities from the Thomas model in the column were in good agreement with the experimental values (Table S5†).

4. Conclusion

In this study, we developed a facile and effective approach for the scalable synthesis of HZO-PVA composite beads based on the simultaneous *in situ* formation of hydrous HZO and cross-linking of PVA chains, which were further functionalized with TETA for effective and selective phosphate sequestration. The PSO kinetic model and Freundlich isotherm could well describe the phosphate adsorption onto HZO-PVA and TETA@HZO-PVA. Compared with HZO-PVA, TETA@HZO-PVA exhibited a superior phosphate adsorption capacity and high selectivity even in the presence of competing anions and DOM. The high and stable phosphate sequestration capacity of TETA@HZO-PVA can be attributed to the combined mechanisms of electrostatic attraction, ligand exchange and Lewis acid–base interactions. Additionally, TETA@HZO-PVA possessed a satisfactory chemical stability during the adsorption process, reaching a high retention of 88.0% even after five consecutive cycles of adsorption. Further, column studies indicated the potential applicability of TETA@HZO-PVA in real wastewater. Taken together, the findings of this study substantiated that *in situ* immobilization of HZO nanoparticles within a simultaneously generated PVA matrix with subsequent surface functionalization can be considered as an effective and facile approach to improve the applicability of HZO for water purification.

Conflicts of interest

There are no conflicts of interest to declare.

Acknowledgements

This study was supported by the Natural Science Foundation of Guangdong Province (2020A1515010856), the Science and Technology Planning Project of Guangzhou City (202102020694), the National Natural Science Foundation of China (52170071, 42177237), the Youth Innovative Talents Project for Innovative Strong Schools of Guangdong Education Department (2019KQNCX109), the Strategic Priority Research Program of Chinese Academy of Sciences (No. XDB40020000), the Science and Technology Planning Project of Guizhou Province (QianKeHeZhiCheng, 2022-217), and the Central Government Leading Local Science and Technology Development QianKeZhongYinDi (20214028). We also thank the Analytical and Testing Center of Guangzhou University for related analysis.

References

1 Y. Zhi, C. Zhang, R. Hjorth, A. Baun, O. W. Duckworth, D. F. Call, D. R. U. Knappe, J. L. Jones and K. Grieger, Emerging lanthanum (III)-containing materials for phosphate removal from water: A review towards future developments, *Environ. Int.*, 2020, **145**, 106115.

2 H. Bacelo, A. M. A. Pintor, S. C. R. Santos, R. A. R. Boaventura and C. M. S. Botelho, Performance and prospects of different adsorbents for phosphorus uptake and recovery from water, *Chem. Eng. J.*, 2020, **381**, 122566.

3 K. Vikrant, K. H. Kim, Y. S. Ok, D. C. W. Tsang, Y. F. Tsang, B. S. Giri and R. S. Singh, Engineered/designer biochar for the removal of phosphate in water and wastewater, *Sci. Total Environ.*, 2018, **616–617**, 1242–1260.

4 B. Wu, J. Wan, Y. Zhang, B. Pan and I. M. C. Lo, Selective Phosphate Removal from Water and Wastewater using Sorption: Process Fundamentals and Removal Mechanisms, *Environ. Sci. Technol.*, 2020, **54**, 50–66.

5 H. Li, Y. Zhao, Z. Xiao, M. Yang and B. Zhou, Analysis on approximate site energy distribution and adsorption behaviors unveils reasons for highly efficient phosphorus removal by a novel sludge-based magnetic gel bead, *Chem. Eng. J.*, 2021, **422**, 130028.

6 M. Silva and J. Baltrusaitis, A review of phosphate adsorption on Mg-containing materials: kinetics, equilibrium, and mechanistic insights, *Environ. Sci.: Water Res. Technol.*, 2020, **6**, 3178–3194.
7 A. Drenkova-Tuhtan, M. Schneider, M. Franzreb, C. Meyer, C. Gellermann, G. Sextl, K. Mandel and H. Steinmetz, Pilot-scale removal and recovery of dissolved phosphate from secondary wastewater effluents with reusable ZnFeZr adsorbent @ Fe_3O_4/SiO_2 particles with magnetic harvesting, *Water Res.*, 2017, **109**, 77–87.
8 W. Huang, Y. Zhang and D. Li, Adsorptive removal of phosphate from water using mesoporous materials: A review, *J. Environ. Manage.*, 2017, **193**, 470–482.
9 Y. Su, H. Cui, Q. Li, S. Gao and J. K. Shang, Strong adsorption of phosphate by amorphous zirconium oxide nanoparticles, *Water Res.*, 2013, **47**, 5018–5026.
10 S. Sonal and B. K. Mishra, A comprehensive review on the synthesis and performance of different zirconium-based adsorbents for the removal of various water contaminants, *Chem. Eng. J.*, 2021, **424**, 130509.
11 L. A. Rodrigues, L. J. Maschio, R. E. da Silva and M. L. da Silva, Adsorption of Cr(VI) from aqueous solution by hydrous zirconium oxide, *J. Hazard. Mater.*, 2010, **173**, 630–636.
12 H. Qiu, C. Liang, X. Zhang, M. Chen, Y. Zhao, T. Tao, Z. Xu and G. Liu, Fabrication of a Biomass-Based Hydrous Zirconium Oxide Nanocomposite for Preferable Phosphate Removal and Recovery, *ACS Appl. Mater. Interfaces*, 2015, **7**, 20835–20844.
13 R. Kumar, S.-J. Kim, K.-H. Kim, S.-H. Lee, H.-S. Park and B.-H. Jeon, Removal of hazardous hexavalent chromium from aqueous phase using zirconium oxide-immobilized alginate beads, *Appl. Geochem.*, 2018, **88**, 113–121.
14 X. Zhao, Y. Zhang, S. Pan, X. Zhang, W. Zhang and B. Pan, Utilization of gel-type polystyrene host for immobilization of nano-sized hydrated zirconium oxides: A new strategy for enhanced phosphate removal, *Chemosphere*, 2020, **263**, 127938.
15 B. Pan, F. Han, G. Nie, B. Wu, K. He and L. Lu, New strategy to enhance phosphate removal from water by hydrous manganese oxide, *Environ. Sci. Technol.*, 2014, **48**, 5101–5107.
16 L. Chen, X. Zhao, B. Pan, W. Zhang, M. Hua, L. Lv and W. Zhang, Preferable removal of phosphate from water using hydrous zirconium oxide-based nanocomposite of high stability, *J. Hazard. Mater.*, 2015, **284**, 35–42.
17 N. Y. Acelas, B. D. Martin, D. Lopez and B. Jefferson, Selective removal of phosphate from wastewater using hydrated metal oxides dispersed within anionic exchange media, *Chemosphere*, 2015, **119**, 1353–1360.
18 T. H. Bui, S. P. Hong, C. Kim and J. Yoon, Performance analysis of hydrated Zr(IV) oxide nanoparticle-impregnated anion exchange resin for selective phosphate removal, *J. Colloid Interface Sci.*, 2021, **586**, 741–747.
19 Y. Shang, X. Xu, S. Qi, Y. Zhao, Z. Ren and B. Gao, Preferable uptake of phosphate by hydrous zirconium oxide nanoparticles embedded in quaternary-ammonium Chinese reed, *J. Colloid Interface Sci.*, 2017, **496**, 118–129.
20 N. Mohammed, N. Grishkewich, H. A. Waeijen, R. M. Berry and K. C. Tam, Continuous flow adsorption of methylene blue by cellulose nanocrystal-alginate hydrogel beads in fixed bed columns, *Carbohydr. Polym.*, 2016, **136**, 1194–1202.
21 L. Zhou, B. He and F. Zhang, Facile one-pot synthesis of iron oxide nanoparticles cross-linked magnetic poly(vinyl alcohol) gel beads for drug delivery, *ACS Appl. Mater. Interfaces*, 2012, **4**, 192–199.
22 Z. Majidnia and A. Idris, Evaluation of cesium removal from radioactive waste water using maghemite PVA–alginate beads, *Chem. Eng. J.*, 2015, **262**, 372–382.
23 W. Zhang, Q. Deng, Q. He, J. Song, S. Zhang, H. Wang, J. Zhou and H. Zhang, A facile synthesis of core-shell/bead-like poly (vinyl alcohol)/alginate@PAM with good adsorption capacity, high adaptability and stability towards Cu(II) removal, *Chem. Eng. J.*, 2018, **351**, 462–472.
24 J. Wan, C. Zhu, J. Hu, T. C. Zhang, D. Richter-Egger, X. Feng, A. Zhou and T. Tao, Zirconium-loaded magnetic interpenetrating network chitosan/poly(vinyl alcohol) hydrogels for phosphorus recovery from the aquatic environment, *Appl. Surf. Sci.*, 2017, **423**, 484–491.
25 Z. Chen, H. Luo and H. Rong, Development of polyaminated chitosan-zirconium(IV) complex bead adsorbent for highly efficient removal and recovery of phosphorus in aqueous solutions, *Int. J. Biol. Macromol.*, 2020, **164**, 1183–1193.
26 Y. Zhao, L. Gai, H. Liu, Q. An, Z. Xiao and S. Zhai, Network interior and surface engineering of alginate-based beads using sorption affinity component for enhanced phosphate capture, *Int. J. Biol. Macromol.*, 2020, **162**, 301–309.
27 W. Zhang, H. Wang, X. Hu, H. Feng, W. Xiong, W. Guo, J. Zhou, A. Mosa and Y. Peng, Multicavity triethylenetetramine-chitosan/alginate composite beads for enhanced Cr(VI) removal, *J. Cleaner Prod.*, 2019, **231**, 733–745.
28 H. Li, Y. Zhang, X. Chen, K. Shi, Z. Yuan, B. Liu, B. Shen and B. He, Synthesis and adsorption aspect of crosslinked PVA-based blood compatible adsorbents for LDL apheresis, *React. Funct. Polym.*, 2004, **58**, 53–63.
29 H. Luo, X. Zeng, P. Liao, H. Rong, T. C. Zhang, Z. Jason Zhang and X. Meng, Phosphorus removal and recovery from water with macroporous bead adsorbent constituted of alginate-Zr(4+) and PNIPAM-interpenetrated networks, *Int. J. Biol. Macromol.*, 2019, **126**, 1133–1144.
30 H. Luo, H. Rong, T. C. Zhang, X. Zeng and J. Wan, Amino-functionalized magnetic zirconium alginate beads for phosphate removal and recovery from aqueous solutions, *J. Appl. Polym. Sci.*, 2019, **136**, 46897.
31 B. Wang, X. Hu, D. Zhou, H. Zhang, R. Chen, W. Guo, H. Wang, W. Zhang, Z. Hong and W. Lyu, Highly selective and sustainable clean-up of phosphate from aqueous phase by eco-friendly lanthanum cross-linked polyvinyl alcohol/alginate/palygorskite composite hydrogel beads, *J. Cleaner Prod.*, 2021, **298**, 126878.
32 M. V. Lopez-Ramon, F. Stoeckli, C. Moreno-Castilla and F. Carrasco-Marin, On the characterization of acidic and basic

surface sites on carbons by various techniques, *Carbon*, 1999, **37**, 1215–1221.

33 J. Sarma and S. Mahiuddin, Specific ion effect on the point of zero charge of α-alumina and on the adsorption of 3,4-dihydroxybenzoic acid onto α-alumina surface, *Colloids Surf., A*, 2014, **457**, 419–424.

34 B. Wang, Y. Zhu, Z. Bai, R. Luque and J. Xuan, Functionalized chitosan biosorbents with ultra-high performance, mechanical strength and tunable selectivity for heavy metals in wastewater treatment, *Chem. Eng. J.*, 2017, **325**, 350–359.

35 X. Dou, D. Mohan, C. U. Pittman and S. Yang, Remediating fluoride from water using hydrous zirconium oxide, *Chem. Eng. J.*, 2012, **198–199**, 236–245.

36 X. Luo, X. Wu, Z. Reng, X. Min, X. Xiao and J. Luo, Enhancement of Phosphate Adsorption on Zirconium Hydroxide by Ammonium Modification, *Ind. Eng. Chem. Res.*, 2017, **56**, 9419–9428.

37 Y. S. Ho and G. McKay, Pseudo-second order model for sorption processes, *Process Biochem.*, 1999, **34**, 451–465.

38 H. N. Tran, S. J. You, A. Hosseini-Bandegharaei and H. P. Chao, Mistakes and inconsistencies regarding adsorption of contaminants from aqueous solutions: A critical review, *Water Res.*, 2017, **120**, 88–116.

39 B. Zhang, N. Chen, C. Feng and Z. Zhang, Adsorption for phosphate by crosslinked/non-crosslinked-chitosan-Fe(III) complex sorbents: Characteristic and mechanism, *Chem. Eng. J.*, 2018, **353**, 361–372.

40 J. Lin, B. Jiang and Y. Zhan, Effect of pre-treatment of bentonite with sodium and calcium ions on phosphate adsorption onto zirconium-modified bentonite, *J. Environ. Manage.*, 2018, **217**, 183–195.

41 H. Xi, Q. Li, Y. Yang, J. Zhang, F. Guo, X. Wang, S. Xu and S. Ruan, Highly effective removal of phosphate from complex water environment with porous Zr-bentonite alginate hydrogel beads: Facile synthesis and adsorption behavior study, *Appl. Clay Sci.*, 2021, **201**, 105919.

42 T. A. H. Nguyen, H. H. Ngo, W. S. Guo, J. L. Zhou, J. Wang, H. Liang and G. Li, Phosphorus elimination from aqueous solution using 'zirconium loaded okara' as a biosorbent, *Bioresour. Technol.*, 2014, **170**, 30–37.

43 J. Wang, X. Tong and S. Wang, Zirconium-Modified Activated Sludge as a Low-Cost Adsorbent for Phosphate Removal in Aqueous Solution, *Water, Air, Soil Pollut.*, 2018, **229**, 47–57.

44 Y. Zhao, L. Guo, W. Shen, Q. An, Z. Xiao, H. Wang, W. Cai, S. Zhai and Z. Li, Function integrated chitosan-based beads with throughout sorption sites and inherent diffusion network for efficient phosphate removal, *Carbohydr. Polym.*, 2020, **230**, 115639.

45 T. Guan, X. Li, W. Fang and D. Wu, Efficient removal of phosphate from acidified urine using UiO-66 metal-organic frameworks with varying functional groups, *Appl. Surf. Sci.*, 2020, **501**, 144074.

46 Y. Wu, X. Li, Q. Yang, D. Wang, Q. Xu, F. Yao, F. Chen, Z. Tao and X. Huang, Hydrated lanthanum oxide-modified diatomite as highly efficient adsorbent for low-concentration phosphate removal from secondary effluents, *J. Environ. Manage.*, 2019, **231**, 370–379.

47 L. Zhang, Q. Zhou, J. Liu, N. Chang, L. Wan and J. Chen, Phosphate adsorption on lanthanum hydroxide-doped activated carbon fiber, *Chem. Eng. J.*, 2012, **185–186**, 160–167.

48 T. Liao, T. Li, X. Su, X. Yu, H. Song, Y. Zhu and Y. Zhang, $La(OH)_3$-modified magnetic pineapple biochar as novel adsorbents for efficient phosphate removal, *Bioresour. Technol.*, 2018, **263**, 207–213.

49 L. Wang, J. Wang, W. Yan, C. He and Y. Shi, $MgFe_2O_4$-biochar based lanthanum alginate beads for advanced phosphate removal, *Chem. Eng. J.*, 2020, **387**, 123305.

50 S. Shan, W. Wang, D. Liu, Z. Zhao, W. Shi and F. Cui, Remarkable phosphate removal and recovery from wastewater by magnetically recyclable $La_2O_2CO_3$/gamma-Fe_2O_3 nanocomposites, *J. Hazard. Mater.*, 2020, **397**, 122597.

51 M. Bourguignon, J. M. Thomassin, B. Grignard, B. Vertruyen and C. Detrembleur, water-borne isocyanate-free polyurethane hydrogels with adaptable functionality and behavior, *Macromol. Rapid Commun.*, 2021, **42**, e2000482.

52 C.-C. Fu, H. N. Tran, X.-H. Chen and R.-S. Juang, Preparation of polyaminated Fe3O4@chitosan core-shell magnetic nanoparticles for efficient adsorption of phosphate in aqueous solutions, *J. Ind. Eng. Chem.*, 2020, **83**, 235–246.

53 S. Dong, Q. Ji, Y. Wang, H. Liu and J. Qu, Enhanced phosphate removal using zirconium hydroxide encapsulated in quaternized cellulose, *J. Environ. Sci.*, 2020, **89**, 102–112.

54 Y. Zhang, B. Pan, C. Shan and X. Gao, Enhanced Phosphate Removal by Nanosized Hydrated La(III) Oxide Confined in Cross-linked Polystyrene Networks, *Environ. Sci. Technol.*, 2016, **50**, 1447–1454.

55 B. Hui, Y. Zhang and L. Ye, Preparation of PVA hydrogel beads and adsorption mechanism for advanced phosphate removal, *Chem. Eng. J.*, 2014, **235**, 207–214.

56 Y. Shi, D. Xiong, Y. Liu, N. Wang and X. Zhao, Swelling, mechanical and friction properties of PVA/PVP hydrogels after swelling in osmotic pressure solution, *Mater. Sci. Eng., C*, 2016, **65**, 172–180.

57 X. Liu and L. Zhang, Removal of phosphate anions using the modified chitosan beads: Adsorption kinetic, isotherm and mechanism studies, *Powder Technol.*, 2015, **277**, 112–119.

58 A. Sowmya and S. Meenakshi, An efficient and regenerable quaternary amine modified chitosan beads for the removal of nitrate and phosphate anions, *J. Environ. Chem. Eng.*, 2013, **1**, 906–915.

59 Y.-Z. Yan, Q.-D. An, Z.-Y. Xiao, S.-R. Zhai, B. Zhai and Z. Shi, Interior multi-cavity/surface engineering of alginate hydrogels with polyethylenimine for highly efficient chromium removal in batch and continuous aqueous systems, *J. Mater. Chem. A*, 2017, **5**, 17073–17087.

60 B. Wang, W. Zhang, L. Li, W. Guo, J. Xing, H. Wang, X. Hu, W. Lyu, R. Chen, J. Song, L. Chen and Z. Hong, Novel talc encapsulated lanthanum alginate hydrogel for efficient phosphate adsorption and fixation, *Chemosphere*, 2020, **256**, 127124.

61 J. Lin, Y. Zhan, H. Wang, M. Chu, C. Wang, Y. He and X. Wang, Effect of calcium ion on phosphate adsorption onto hydrous zirconium oxide, *Chem. Eng. J.*, 2017, **309**, 118–129.

62 Q. Q. Zhong, L. Shen, Y. Q. Zhao, Y. C. Hao, L. C. Meng, Y. J. Liu, X. Xu, Y. N. Shang, B. Y. Gao and Q. Y. Yue, Preferential capture of phosphate by an Enteromorpha prolifera-based biopolymer encapsulating hydrous zirconium oxide nanoparticles, *Environ. Sci. Pollut. Res.*, 2021, **28**, 34584–34597.

63 Z. A. Sutirman, M. M. Sanagi, K. J. Abd Karim, W. A. Wan Ibrahim and B. H. Jume, Equilibrium, kinetic and mechanism studies of Cu(II) and Cd(II) ions adsorption by modified chitosan beads, *Int. J. Biol. Macromol.*, 2018, **116**, 255–263.

64 W. Xiong, J. Tong, Z. Yang, G. Zeng, Y. Zhou, D. Wang, P. Song, R. Xu, C. Zhang and M. Cheng, Adsorption of phosphate from aqueous solution using iron-zirconium modified activated carbon nanofiber: Performance and mechanism, *J. Colloid Interface Sci.*, 2017, **493**, 17–23.

65 Q. Sun, L. Zhu, B. Aguila, P. K. Thallapally, C. Xu, J. Chen, S. Wang, D. Rogers and S. Ma, Optimizing radionuclide sequestration in anion nanotraps with record pertechnetate sorption, *Nat. Commun.*, 2019, **10**, 1646.

